Mechanochemical Synthesis of Hydraulically Reactive Calcium Silicate Minerals via Thermally Assisted Mechanical Grinding

Van Son Nguyen[a], Elsa Qoku[b], Khoa Nhan Mai[a], Dominik N. Groh[a], Jacob A. DeWitt[a], Kimberly E. Kurtis[b, c*], Carsten Sievers[a, d, e*]

[a] School of Chemical & Biomolecular Engineering, Georgia Institute of Technology, Atlanta, Georgia 30332, United States
[b] School of Civil and Environmental Engineering, Georgia Institute of Technology, Atlanta, Georgia 30332, United States

[c] School of Materials Science and Engineering, Georgia Institute of Technology, Atlanta, Georgia 30332, United States
[d] School of Chemistry & Biochemistry, Georgia Institute of Technology, Atlanta, Georgia 30332, United States
[e] Renewable Bioproducts Institute, Georgia Institute of Technology, Atlanta, Georgia 30332, United States

***Corresponding author:** kkurtis@gatech.edu; carsten.sievers@chbe.gatech.edu

Keywords: Calcium Silicates, High-temperature ball milling, Mechanochemistry, Cementitious materials, Process Integration

Abstract

This study explores a thermally assisted mechanochemical approach alternative to conventional cement synthesis as a potential to produce hydraulically reactive calcium silicate phases. Ball milling of mixed CaO/SiO_2 feedstocks at temperature ranges 100-300 °C increases the formation of the Ca-O-Si bonds and precursor reactivity. Spectroscopic analyses (FTIR, MAS-NMR, UV-Vis DRS) indicate increasing amorphization with milling temperature, attributed to improved mixing and thermally assisted diffusion. Upon hydration, all treated samples exhibit exothermic heat release, with the sample prepared at 300 °C showing the most pronounced reactivity. Thermal analysis reveals weight loss consistent with C-S-H formation, confirming cement-like behavior. In summary, moderate thermal input during milling promotes structural activation and enhances downstream hydraulic reactivity, providing a proof-of-concept for energy-reduced cement precursor processing.

1. Introduction

Cement production significantly contributes to global CO_2 emissions, accounting for approximately 5-6%.[1] These emissions arise primarily from the calcination of limestone ($CaCO_3$ to CaO) and the intense thermal energy required to drive clinker formation, which occurs at temperatures exceeding 1400 °C in rotary kilns.[2-4] In particular, the formation of hydraulic calcium silicate phases, most notably tricalcium silicate (C_3S) and dicalcium silicate (C_2S) requires extreme thermal input and significant fuel consumption, leading to a high energy demand and carbon intensity.

During the process of cement production, lime is combined with clay and shale, rich in SiO_2 and Al_2O_3 (mainly γ- and δ-Al_2O_3), along with sand, leading to the formation of mixed oxide phases of hydraulically reactive calcium silicate, aluminate and ferrite phases.[5-7] The calcination reaction occurs at a temperature between 800-900 °C, whereas the exothermic reactions involving CaO, Al_2O_3, SiO_2 and Fe_2O_3 to form C_2S, tricalcium aluminate (C_3A) and calcium ferrite (C_4AF) take place in the temperature range from 800 – 1300 °C. The reaction for the formation of the main hydraulic component of tricalcium silicate (C_3S), that is the most abundant phase of Portland cement (~60 wt.%) typically occurs at temperatures exceeding 1400 °C. On the cooling from elevated temperatures, C_3S exhibit 7 polymorphs. All polymorphs have similar structures, mainly distinguished by small distortion as the C_3S structure accommodates crystallographic strain during the cooling below its limit of stability. The

monoclinic polymorphs M_I-M_{III} are often found in Portland cement. Dicalcium silicate (C_2S) as well exhibits a number of polymorphs with β-C_2S being the hydraulic relevant polymorph.[8]

Efforts have been made to enhance energy efficiency in cement kilns. These include implementing heat recovery systems, such as the application of organic Rankine cycle (ORC) or Kalina cycle to recover heat from the cement production,[9, 10] or the optimization of process control, for instance, improving operational parameters, i.e., gas and electrical power management,[11] energy balance and reaction kinetic monitoring,[12] and plant integrations.[2] Furthermore, alternative clinker production methods, such as low-temperature calcination processes and novel binder materials, are being investigated to reduce energy consumption during clinker formation.[13] Consequently, alternative synthesis pathways for cementitious materials that operate at lower temperatures and minimize fossil energy input are of increasing interest.

Mechanochemistry offers an alternative and relatively less explored approach compared to processing solids by grinding or impacting. In addition to solid state mixing, it creates highly reactive transient domains on solid surface that can be explained as intense strain or thermal hot spots.[14-16] Tricker et al. demonstrated the decomposition of $CaCO_3$ by ball milling under nominally ambient conditions and rationalized the observed reactivity with transient hotspots exceeding 800 °C due to high intensity mechanical impacts.[17] In addition, the formation of highly strained environments is responsible for extraordinary reactivity in many cases.[18, 19] Moreover, the constants formation and sintering of surfaces offers a promising prospect for improving energy efficiency of processes that require the reaction between two or more solids. Mechanochemistry has been implemented in the synthesis and processing of multiple solid inorganic oxides, especially in the field of doped metal-oxides, most notably with Al or Mn-doped ZnO,[20-23] and SnO_2,[24] or tertiary metal-oxides, such as $Ca_2Mn_3O_8$,[25] $CaMn_2O_4$, and $CaMnO_3$.[26]

In the field of cement science, some studies have demonstrated mechanochemical formation of mixed metal oxide phases, but none have systematically explored the role of moderate external heating during the milling process itself. Chen demonstrated the conversion of $CaCO_3$ and amorphous Al_2O_3 to $CaO{\cdot}Al_2O_3$ (CA) through high-energy ball milling and subsequent annealing, showing the reduction of the required temperature for subsequent calcination compared to conventional methods (i.e., ~1335 °C) by at least 100 °C.[27] Mi et al. also illustrated the feasibility of synthesizing dicalcium silicate from a CaO/SiO_2-gel mixture using ball milling at room temperature from 30 minutes up to 5 hours followed by a heat treatment process at up to 900°C.[28] Ettringite ($[Ca_3Al(OH)_6]_2{\cdot}(SO_4)_3{\cdot}26H_2O$), a both a naturally occurring mineral and a product of cement hydration, was synthesized using wet milling at ambient temperature.[29] The synthesis of these materials required long milling times (> 5 h). While the synthesis of cementitious materials has demonstrated success, the long milling times needed to achieve moderate yields and the need for subsequent high temperature treatments are significant barriers to further development.[30] Conventional ball milling can induce the formation of nanoscale composite structures, wherein chemical reactions are initiated at the grain boundaries of adjacent reactant phases, significantly enhancing reaction kinetics through phenomena, such as reduced diffusion length (via grain fracturing), decreased activation energy (resulting from the generation of surface defects and radicals), and the creation of fresh reactive surfaces (due to continuous surface restructuring).[22] However, the reaction is often incomplete when milling occurs at or near room temperature. Consequently, post-milling heat treatment is frequently required to achieve full reaction completion.[22] Reasons can include the kinetic limitation, due to temperature difference between the local and the solid bulk,[31] and insufficient mixing and inadequate contact between reactants leading to limited number of reaction sites.[32] The coupling of mechanical stress and thermal energy could potentially improve solid-state diffusion, enhance precursor mixing, and promote amorphization or nanostructuring that facilitate downstream hydration. More recent work has broadened the use of mechanochemical activation in cement systems, for example by enhancing the pozzolanic reactivity of clays, industrial by-products, and slags through high-energy milling and alkanolamine-assisted grinding, enabling high clinker substitution while maintaining or improving mechanical performance.[33-37] However, these studies still

rely on ambient-temperature milling and/or post-milling calcination or hydration, and do not systematically investigate the effect of controlled, moderate external heating during the milling step itself, which is the focus of the present work.

In this work, the primary goal is to develop a strategy for an energy-efficient synthesis of hydraulically reactive calcium silicate phases, in which mechanical grinding at moderate temperatures significantly improves the amorphization, Ca-O-Si bond formation, and hydraulic reactivity. To realize this concept, a novel milling vessel concept of thermal-assisted mechanical grinding was developed allowing for controlled temperature regulation, up to 300°C. While equipment limitation restricted the operating range to 300°C, extrapolation of the results successfully demonstrated the system's potential in lowering the processing temperature of cement kilns.

2. Materials and Methods

2.1 Materials

Quartz sand (SiO_2) 0.5-10 μm (~99%) was supplied by Sigma-Aldrich. Calcium oxide (CaO), reagent grade, was purchased from Alfa Aesar. Pure monoclinic (M_{III}) C_3S was purchased (from Wŭsh, Research Institute of Building Materials, Czech Republic) was used as a reference material. The anhydrous phase had a d_{50} particle size of 9.02 μm and was of high purity as indicated from the Rietveld refinement (see Supplementary Information). All chemicals were handled as received without further purification.

2.2 Mechanochemical Synthesis of the Calcium Silicate Minerals at Elevated Temperatures

Milling experiments were conducted using a Retsch MM500 shaker mill with a pill-shaped stainless-steel vessel and grinding balls. (Figure 1a-b) The employed reactor vessel had an internal volume of 25 mL. In all experiments, ten grinding balls, each 10 mm in diameter and weighing approximately 4.04 g, were used. Approximately 1 g of solid reagents was loaded into the vessel before starting the experiment. The vessel was sealed with a 1″ PTFE O-ring after loading, and the headspace gas inside the vessel remained air. The vessel was wrapped with a heating tape and a thermal element, secured with aluminum tape. (Figure 1c) Three layers of commercial aluminum foil were wrapped around the outside to prevent damage and heat loss. The vessel was then placed inside a stainless-steel mantle, which was sealed to prevent heat loss. (see Figure 1c) The heating element is then connected to a thermal controller allowing the control of the environment temperature of the reaction. Compressed air is provided into the milling chamber to prevent overheating. In all experiments, approximately 0.74 g (0.0132 mol) of CaO and 0.264 g (0.0044 mol) of SiO_2 were used to achieve the optimal stoichiometric ratio of C/S of 3:1. The syntheses were performed at room temperature (approximately 20°C), 100 °C, 200 °C, and 300 °C at 20 Hz for one hour. After the reaction, the solid reaction products were retrieved, and the vessel was cleaned by ball-milling approximately 0.5 g silica-alumina powder using the original ball and vessels configuration before being sonicated for 30 minutes and dried in a 103 °C convection oven.

2.3 Characterization Methods

Particle size measurement

The particle size distribution (PSD) was determined with a Wyatt DynaPro NanoStar dynamic light scattering detector. For this, approximately 10-15 mg of the samples were dispersed in 1 mL methanol inside a 15 ml test tube using the vortexer before inserting into the laser chamber. Each sample was measured ten times, with each measurement having a duration of 10 seconds.

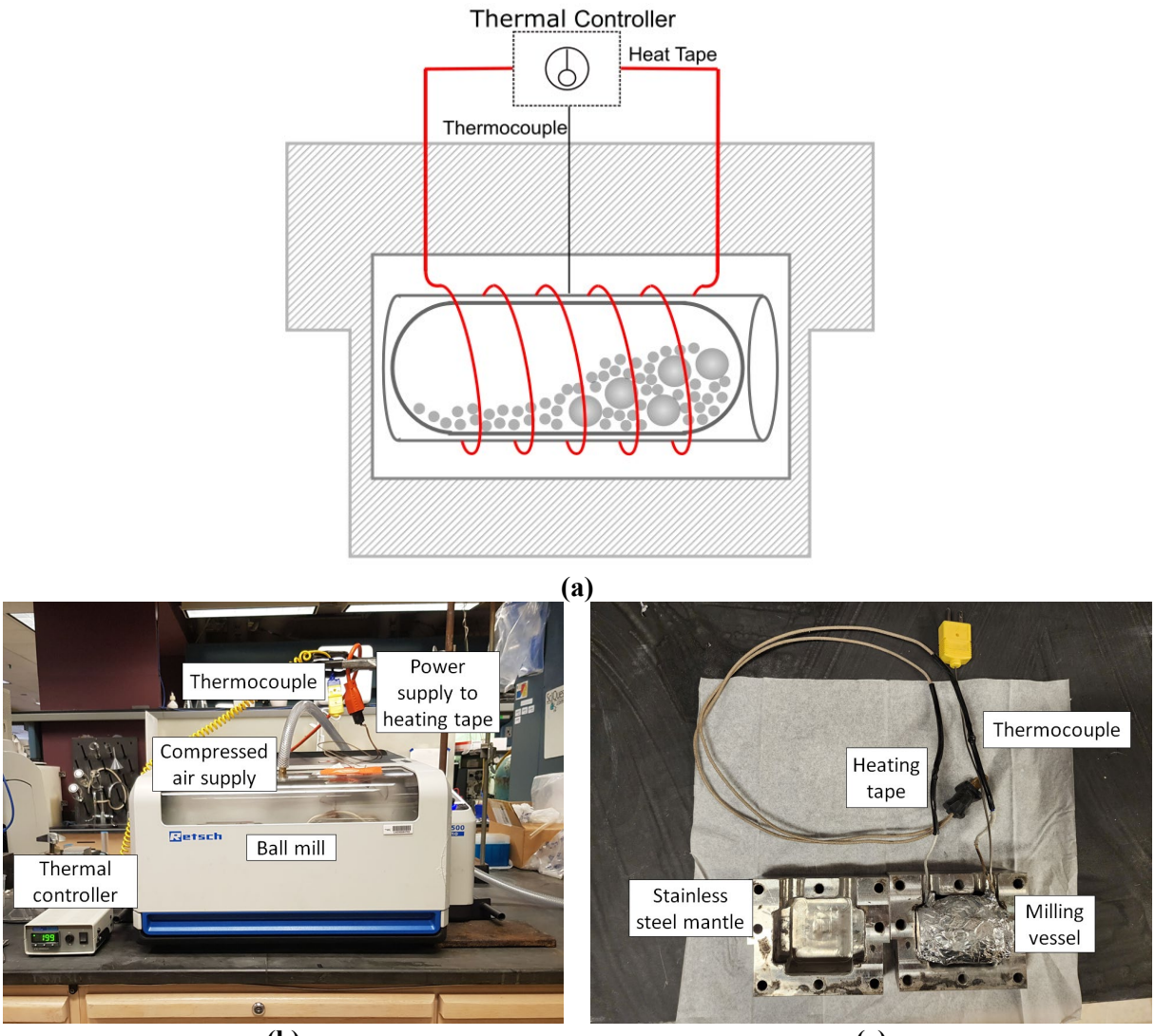

Figure 1: Setup for mechanochemical reactions at elevated temperature: **(a)** Schematic representation **(b)** Photo of the experimental setup **(c)** Close-up on the vessel and mantle.

Spectroscopy

ATR-FTIR spectra were measured with the Thermo Scientific™ iS50 FTIR spectrometer equipped with Smart iTR™ Attenuated Total Reflection (ATR) sampling accessory with a ZnSe crystal as internal reflection element (IRE). Each sample, weighing a few milligrams, was mounted on the IRE and firmly held in place using the ATR stage clamp. The spectra were obtained across the wavenumber range of 700 cm^{-1} to 4000 cm^{-1}, with 64 scans per sample.

MAS-NMR spectroscopy measurements for the ^{29}Si nucleus were performed on a Bruker Avance III 400 MHz spectrometer with a spinning frequency of 10 kHz. For the all samples, a recycle delay (d1) of 20 s was used with the resonance of 79.569 MHz and 3072 scans in reference to 3-(Trimethylsilyl)-1-propanesulfonic acid sodium salt.

UV-Vis DRS spectra were collected using the Thermo Scientific™ Evolution 300 spectrophotometer equipped with a Praying Mantis™ Diffuse Reflection Accessory. Roughly 10 mg of the solid sample was loaded into the holder cup. The upper surface was flattened before each measurement. All spectra were collected across the wavelength region of 190 nm to 500 nm, with the scan speed of 60 nm per minute.

Annealing
The milled samples were annealed under 200 ml/min air flow at 1000 °C for 2 h in an RS 80/750/11 Nabertherm tube furnace with the temperature ramp rate of 10 K/min. The annealed amount for each sample was approximately 50 mg. The samples were left for passive cooling to room temperature without the influence of active quenching.

X-ray powder diffraction
The crystalline phases were evaluated for each sample by X-Ray Diffraction using a Rigaku MiniFlex600 powder X-ray diffractometer with a CuKα (λ = 1.54 Å) radiation source. The operating conditions were 30 kV and 15 mA. Each measurement was taken with a scan speed of 10° per minute and a step size of 0.01°. Phase identification was carried out by using X'Pert HighScore Plus software equipped with a PDF-4 database (ICDD) with a purchased license from IMS Materials Characterization Facility.

Scanning electron microscopy (SEM) and elemental analysis via Energy-dispersive X-ray spectroscopy (EDX)
SEM-EDX analyses were performed simultaneously with a Thermo Scientific™ Axia™ ChemiSEM™ instrument equipped with a tungsten filament source and a coupled TrueSight EDX detector. SEM imaging of the samples was conducted using an Everhart–Thornley detector (ETD) with a working distance of 9.4–10.4 mm under high vacuum conditions and an accelerating voltage of 10.00 kV. EDX spectra of the samples were acquired simultaneously with a minimum scan time of 60 seconds, enabling quantitative elemental mapping and compositional analysis. EDX analyses were repeated three times for each sample. A small quantity (a few milligrams) of each sample was deposited onto a double-sided carbon tape attached to the designated holder in its powdered form, without undergoing any additional polishing steps.

Thermogravimetric (TGA) and Differential Scanning Calorimetry (DSC) Analysis
TGA and DSC analyses were done using the DSC-TGA Q series 600 using the loading of approximately 10 mg into an alumina crucible. The temperature ramp was set to 20 K/min increasing to 1200 °C under the 100 mL/min flow of N_2 as headspace gas for all measurements.

Isothermal Calorimetry
Isothermal calorimetry measurements were performed on a TAM air isothermal calorimeter by Thermometric TA Instruments to examine hydration behavior of the mechanochemical synthetized samples. A relatively small amount of the dry powder (~0.5 g) was mixed with water at a water-to-solid ratio of 1 and placed in small ampules in the calorimeter Measurements were carried out at 23 °C for 47 hours.

Thermogravimetric Analysis (TGA) for hydrated samples
TGA was performed using a TG/DTA7300 instrument by Hitachi Thermal Analysis System – at 47 hours after mixing with water. During the measurements a gas flow rate of 100 ml/min of inert nitrogen was used for the samples with the following hear profile: Samples were held at 40 °C for ~ 1.5 hours, until the water evaporation was complete. The sample temperature was then raised at a rate of 10 °C/min up to 1000 °C.

3. Results and Discussion

3.1 Probing structural changes with spectroscopy

To investigate the effect of temperature on the evolution of CaO/SiO_2 mixtures during milling, a combination of spectroscopic techniques including ATR-FTIR, ^{29}Si MAS-NMR, and UV-Vis diffuse reflectance spectroscopy was employed. These methods offer insight into local bonding environments and short-range order that are not readily accessible through conventional diffraction techniques.

Figure 2 shows the ATR-FTIR spectra of the CaO and SiO_2 mixtures milled at different temperatures. For comparison, the anhydrous monoclinic M_{III} form of tricalcium silicate, C_3S, as the predominant mineral phase commonly found in Portland cement was also analyzed. In all spectra, the characteristic

bands corresponding to the Si-O-Si stretching vibrations were observed in the 1160 to 1010 cm^{-1} region.[38] Bands at 800-783 cm^{-1} can be attributed to the Si-O stretching modes of terminal Si-OH groups.[39] As milling progressed, two bands corresponding to the presence of inorganic CO_3^{2-} were observed at 1474-1420 cm^{-1} and 875 cm^{-1}.[38, 40] The presence of $CaCO_3$, detected by FTIR spectroscopy and confirmed by TGA, is attributed to carbonation of CaO during or immediately after milling when exposed to ambient air. The band at 910-940 cm^{-1} was assigned to the Ca-O-Si stretching mode of the calcium-silicate.[38, 41, 42] This region was dominant in the spectrum of the monoclinic anhydrous C_3S. The increasing intensity of this band with increasing process temperature suggests that calcium silicate

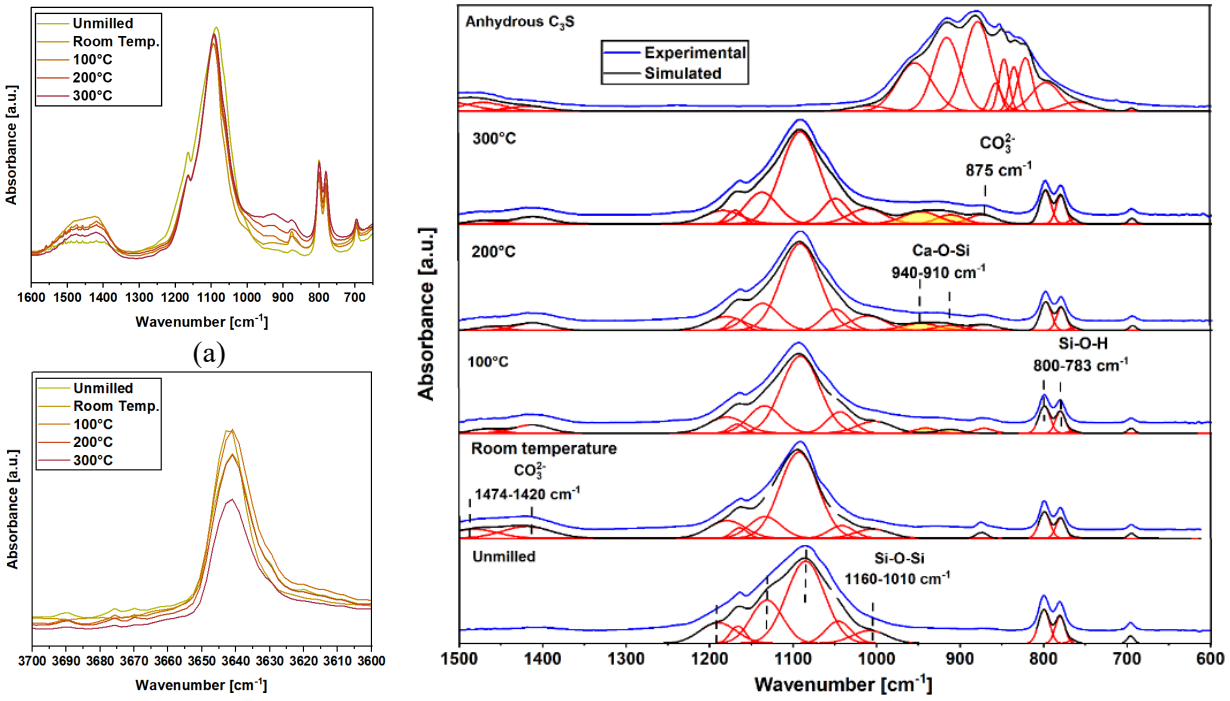

Figure 2: ATR-FTIR analysis of CaO/SiO_2 mixtures milled at various temperatures: (a) Fingerprint region spectra (650-1600 cm^{-1}), (b) OH-stretching region spectra (3600–3700 cm^{-1}) and (c) Gaussian peak deconvolution of the fingerprint region comparing unmilled and samples milled at different temperatures with reference to monoclinic C_2S. Experimental spectra (blue), simulated fits (black), and individual Gaussian components (red) are shown. Key vibrational bands (e.g., Si-O-Si, Ca-O-Si, CO_3^{2-}, Si-OH) are labeled.

phases form, particularly as the temperature increases to 200 and 300 °C.

Figure 3 presents the ^{29}Si MAS-NMR spectra of CaO and SiO_2 mixtures milled at different temperatures and the reference monoclinic anhydrous C_3S. The spectrum of the unmilled sample was dominated by a strong resonance centered at ~ -109 ppm. This resonance has been assigned to the presence of quartz (Q^4 sites) in the mixtures.[43] The peak became much broader with milling and increasing temperature, thus suggesting amorphization of SiO_2 during the different treatments. This observation is in good agreement with the XRD patterns of the as-milled samples (*vide infra*), where a decrease in crystallinity was observed with the increase of the temperature (Figure 5a). In the samples with higher milling temperatures, a shift toward lower coordinated Si was observed with the growth of broad shoulder/tails in the region of -90 to -100 ppm of Q^3-Si, -75 to -93 ppm of Q^2-Si, -70 to -83 ppm of Q^1-Si, and -60 to 81 ppm of Q^0-Si.[43] More specifically, for the sample milled at room temperature, broad resonances were observed near 69, -82 and -91 ppm. As the processing temperature increased, additional broad shoulders/tails became evident with the most prominent ones centered ~-75, -85 ppm and ~-91 ppm.

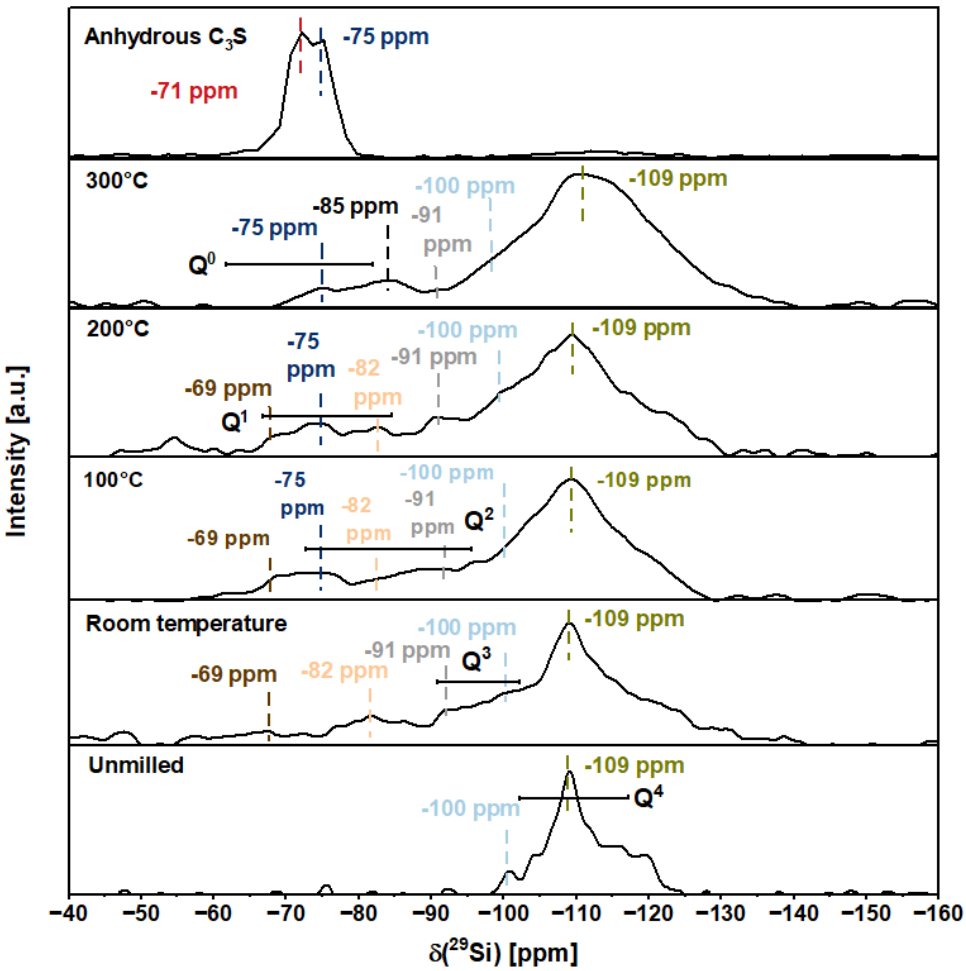

Figure 3: ^{29}Si MAS-NMR spectra of the CaO/SiO_2 mixture milled at different environment temperatures and the monoclinic C_3S. Assignment of chemical shift ranges were adapted from Walkley et al. [43]

The ^{29}Si MAS-NMR spectrum of the pure monoclinic C_3S is included for comparison and exhibited a typical line shape observed for this type of polymorph.[44] As indicated in Figure 3, two main resonances centered at -71 and -75 ppm were identified. ^{29}Si MAS NMR spectra of synthetic samples of M_{III} alite and β form of belite, exhibited resonances in the range from -66 to -78 ppm. The broadened line shape of the alite spectra contains contribution of 18 different resonances from SiO_4 tetrahedra in the Q^0 environment and the resonances for all these sites cannot be resolved even for the synthetic M_{III}. Triclinic polymorph of C_3S exhibits 9 different resonances in the range from -69 to 74 ppm. On the other hand, dicalcium silicate polymorphs exhibit single resonances at -71.1, -71.3 and -73.7 ppm for α, β, γ structures, respectively,[45] while pseudo-wollastonite exhibits isotropic chemical shifts (Q^2) around -83.6 ppm.[45] Due to the broadness of the resonances, a clear unambiguous identification of the individual phases mentioned above cannot be made. However, the presence of the shoulders/tails in the same region suggests chemical modification of the mixture. This is attributed to the formation of amorphous Ca-Si-O domains during the thermal-assisted ball milling process. Taken together, the ATR-FTIR (Figure 2) and ^{29}Si MAS-NMR (Figure 3) spectra demonstrate an increasing formation of Ca-O-Si bonds with rising milling environment temperature. Specifically, a shift from predominantly Q^4 tetrahedral Si in the unmilled sample to a mixture of Q^1, Q^2, and Q^3 Si, with oxygen-bridged Ca, with the rising temperature and the appearance of new FTIR bands suggest enhanced amorphization of SiO_2 and incorporation of Ca into the silicate framework. These findings indicate that elevated temperature during milling positively influences the development of Ca-O-Si bonds.

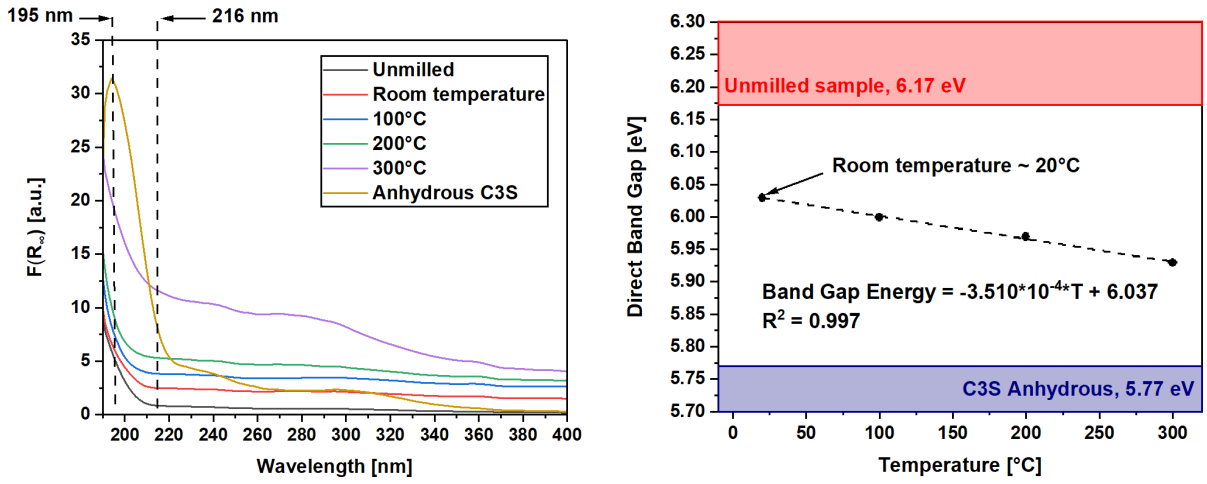

(a) (b)

Figure 4: (a) UV-Vis DRS spectra of the CaO/SiO_2 mixture milled at different environment temperatures and the monoclinic anhydrous C_3S expressed as Kubelka-Munk function (b) Evolution of the direct band gap as a function of the milling environment temperature.

Figure 4a illustrates the UV-Vis DRS spectra of the CaO and SiO_2 mixtures milled at different temperatures in reference to the anhydrous C_3S with a focus on the wavelength region of between 190 and 400 nm expressed as the Kubelka-Munk function (See Section SIV.1). The corresponding characteristic direct band gap of each sample was determined using the Tauc method (Figure S10).[46] The evolution of direct band gap with the milling temperature is illustrated in Figure 4b. The absorption of the UV region shows the excitation of the electrons from the bonding to non-bonding (i.e. higher energy) orbital. In an alkali earth oxide like CaO, the bonds between molecules are ionic (donated e^- from Ca^{2+} cations) whereas with the SiO_2 they are covalent. Thus, the dislocation of the valence electrons in the Ca and O atoms results in poor absorption of UV radiation as well as a large band gap. However, once the Ca-O-Si bonds are formed, the transition towards the ionic-covalent properties of the samples can result in much higher absorption of UV light. The characteristic band position for monoclinic anhydrous C_3S was determined as 195 nm. Thus, the increased absorption of UV radiation in the lower wavelength region with increasing temperature during milling indicated that the substitution of Ca-O-Ca ionic bonds within the CaO lattice with Ca-O-Si polar covalent bonds was facilitated.

Collectively, these spectroscopic results indicate that moderate thermal input during milling promotes the breakdown of crystalline SiO_2 and the formation of Ca-O-Si linkages.

3.2 Phase Development during Annealing

Having established that thermally assisted milling promotes amorphization and Ca-O-Si bond formation, we next investigated whether these structural precursors facilitate crystalline calcium silicate phase formation upon annealing. For this purpose, milled samples were annealed at 1000 °C for 2 hours in air and subjected to passive cooling without quenching. The resulting XRD patterns are shown in Figure 5. Upon mechanical impact and annealing, the diffractions corresponding to the SiO_2 crystals became nearly undetectable, but a considerable amount of CaO was still detected, as indicated by its characteristic diffraction pattern. The higher the temperature during milling, the less significant the diffraction intensity from the CaO crystals, indicating that CaO was increasingly incorporated in calcium silicate phases. The formation of these phases was facilitated with increasing structural disorder introduced during milling. XRD patterns of the as-milled samples, shown in Figure 5a, exhibited significant intensity reduction with increasing milling temperature. These changes suggest progressive amorphization of the starting CaO and SiO_2 components, likely due to repeated impact-induced stress

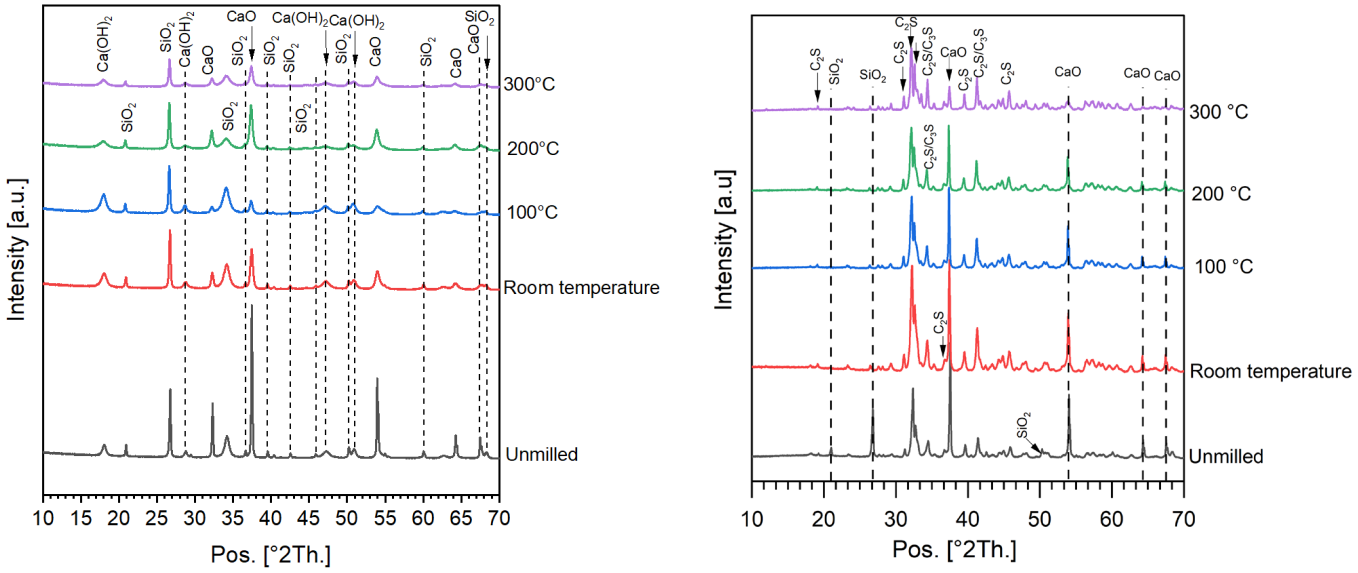

Figure 5: XRD patterns of the CaO/SiO_2 mixture milled at different environment temperatures a) before and b) after annealed at 1000 °C for 2 h.

and enhanced solid-state mixing. Although no discrete calcium silicate phases were detected in the as-milled mixtures, the formation of amorphous mixed metal oxide domains is supported by the spectroscopic evidence presented and supports the hypothesis that milling facilitates early-stage transformation into reactive precursor domains.

The presence of $Ca(OH)_2$ in the starting material was confirmed via the DSC results (*vide infra*), the TGA results (Figure S3), and ATR-FTIR spectra (Figure 2 and S4-S8). Specifically, an endothermic peak in the range of 375-475 °C in both as-mixed and milled samples is attributed to $Ca(OH)_2$ decomposition. The mass loss in TGA from 400 °C supports this assignment to dehydration. The diminishing intensity of the OH-stretching band at 3640 cm^{-1} in ATR-FTIR spectra (Figure 1b) over the milling period corroborates the corresponding reduction in diffraction peak intensity characteristic of the portlandite, i.e., $2\theta = 18.0°$, 28.7°, and 50.8°.

The formation of the calcium silicate has been reported to be heavily diffusion limited.[47] This is one of the reasons for the high temperature required in cement kilns. By elevating the temperature and employing intense mixing during milling, it is possible to ensure effective diffusion without necessitating the extremely high temperatures characteristic of a cement kiln. The major calcium silicate phase identified in the milled samples (room temperature up to 300 °C) was the polymorph β-C_2S (larnite), with major diffraction peaks centered between 32.03 and 34.38° 2θ. Besides β-C_2S polymorphs, additional traces of monoclinic C_3S (51.67° 2θ) severely overlapping with those of C_2S were also identified. The intensity of this peak was slightly stronger for the sample milled at 300 °C. In the CaO/SiO_2 mixture milled at 300 °C the presence of CaO was observed but almost no SiO_2 diffraction peaks. The same applies to the samples milled at 200 °C and 100 °C, whereas small traces of SiO_2 were identified in the sample milled at room temperature. Mi et al. showed the presence of a minimal amount of C_2S in the mixtures of calcium oxide and silica gel milled at room temperature for 30 minutes or more after annealing at least 600 °C. The polymorph of C_2S formed was not specified in their work.[28] In their study, significant diffraction peaks were observed only after milling for 2 h or longer with the annealing temperature of 900 °C. The present work showed that an increased temperature within the milling vessel facilitates the emergence of prominent characteristic peaks corresponding to C_2S and C_3S phases during the subsequent annealing step (Figure 5b). Finally, in the sample milled at 300 °C, a calcium-ferrite phase, with a peak centered around $2\theta = 12.01°$ and 33.5° was identified. This is

attributed to the formation of steel shavings from the milling vessel and their reaction with the feedstock during the milling process.

3.3 Thermal behavior of thermo-mechanically activated samples

While XRD reveals phase development after annealing, DSC of as-milled powders provides insight into how structural disorder introduced during milling influences their thermal behavior prior to crystallization. By comparing thermal responses across different milling temperatures, it becomes possible to correlate the extent of structural reorganization during milling with the observed phase evolution during annealing.

The first endothermic peak, observed between 375 °C and 475 °C in both the as-mixed and milled samples, is attributed to the decomposition of $Ca(OH)_2$ (Figure 6). [28] Its diffraction was observed in the XRD pattern (Figure 5a). The decrease in mass observed in the TGA commencing at 400 °C (Figure S3) corroborated the assignment of the endothermic peak to a dehydration reaction. A significant exothermic region between 475 °C and 1000 °C is due to the heat of crystallization emitted from thermally induced crystal restructuring.[28] An increase in exothermic behavior above 1000 °C is attributed to the reaction between CaO and SiO_2.

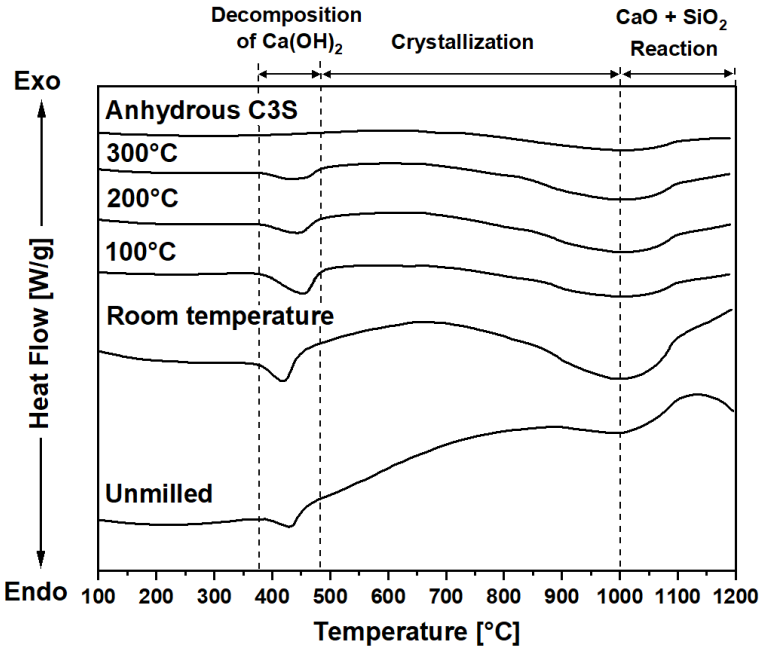

Figure 6: DSC curves of the CaO/SiO_2 mixture milled at different environment temperatures and the anhydrous C_3S reference.

For the samples that were milled at higher temperature, the endothermic peak corresponding to the $Ca(OH)_2$ decomposition was less pronounced. This suggests that the higher milling temperature promotes the dehydration process of the portlandite phase from the starting material. The reduction in heat flow intensity in the exothermic region between 475 °C and 1000 °C for samples with higher milling temperatures suggests that the formation of the amorphous calcium silicate minerals already occurred during milling. Furthermore, it is suggested that ball-milling caused significant stress on the lattice through impact, leading to structural distortion of the impacted domains.[22] During milling, frequent impact and shear forces increase the interactions and contacts between the grain boundaries of the reactant phases, promoting their adjunction and the homogenization of the reaction mixture. Milling reduces the crystallization potential by disrupting the order of the crystal structure, leading to a more disordered material with diminished ability to crystallize. As a result, the milled samples exhibit a lower exothermic response during heating, reflecting the reduced tendency for crystal growth compared to the

unmilled samples. The reduced exothermic behavior in the higher temperature region (above 1000 °C) for samples milled at higher temperatures indicates the partial conversion of the starting material to calcium silicate during milling, with additional phase transformations potentially occurring during cooling. In other words, some of the calcium silicate phases already formed during the milling treatment. The enhanced conversion of the $Ca(OH)_2$ to form CaO and H_2O, followed by the reaction of CaO with SiO_2 explain the decrease in the XRD diffraction intensity at higher temperatures.

3.4 Morphological Changes of Thermo-Mechanically Activated CaO/SiO_2 Samples

The morphological changes of the processed CaO/SiO_2 mixture were examined by SEM-EDX (Figure 7), as morphological evolution of the powders during milling also plays a critical role in reactivity. Larger and bulkier particles were observed in the mixed samples (Figure 7a). Figure 7b illustrates both the fragmentation and agglomeration of particles during milling. While the particles were finer, they also tended to form large aggregates. EDX imaging and spectra showed a clear distinction between two solid phases before grinding and improved homogeneity with no clear material separation thereafter. (Figure S11-S13) The average atomic ratio of Ca/Si for each sample was determined as 3.132 ± 0.369,

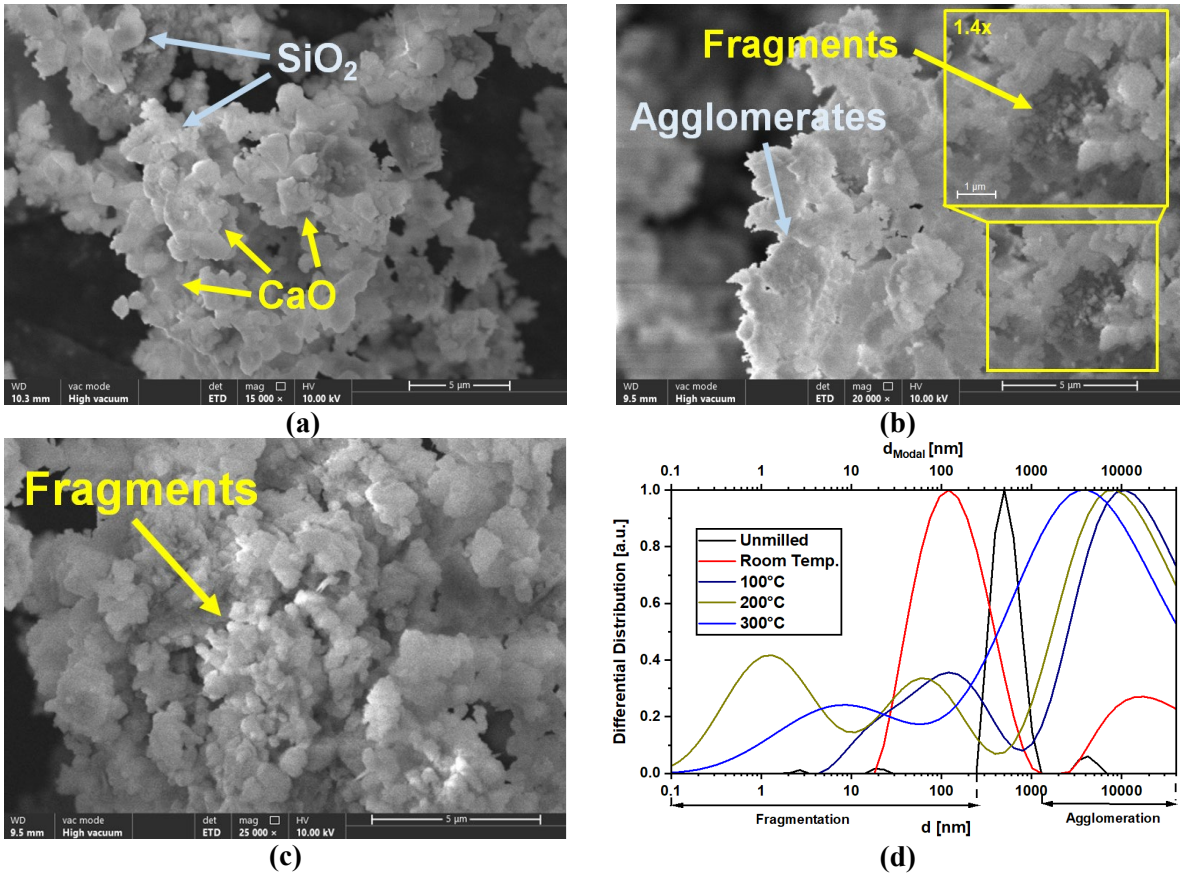

Figure 7: SEM images of the of the CaO/SiO_2 mixture (a) unmilled with grain boundaries are marked in yellow for CaO and blue for SiO_2, (b) at room temperature with a 1.4 x zoom window for better illustrations of particle fragments, (c) fragments at 100°C and (d) PSD of CaO/SiO_2 samples milled at different temperatures.

with a relatively narrow distribution showing good material balance during the process (FigureS14). The PSD (Figure 7d) showed that under the influence of the elevated milling environment temperature both the fragmentation and the agglomeration of the particles are possible. There was a shift from the unimodal distribution with the modal diameter of the particle of approximately 0.5 µm to a multi-modal distribution with the modal diameters of 0.12, 10.93, 8.62, and 4.23 µm, when the samples were milled at room temperature, 100 °C, 200 °C, and 300 °C, respectively. The rise in oversized particles during the milling process can be attributed to the sintering process. The change in the particle size during milling influences the post-processing requirements of the material. The particle size has an effect on

the reactivity as well as the overall strength of the produced cement, as a larger surface area can enhance their reactivity during hydration, which leads to improved early-age strength development in cementitious materials.[48-50] Further mechanical processing, such as grinding and sieving, or use of chemical grinding aids (e.g,. alkanolamines)[51] might therefore be required.

3.5 Investigation of the hydraulic reactivity of thermo-mechanically activated powders

To assess the cementitious activity in thermo-mechanically activated samples, a hydration study was conducted on the treated samples. Figure 8 shows the heat flow calorimeter of the samples mixed with water. The first peak (Figure 8a), in the very first minutes of the contact with water, corresponds to the reaction of CaO with water and additional formation of $Ca(OH)_2$. In the timespan from 2 to 10 hours (Figure 8b) an additional release of heat was observed for all mixtures, except for the unmilled sample. The mixture treated at 300 °C exhibited the largest heat release, followed by the samples milled at 200 °C, 100 °C and room temperature. This occurrence suggests a hydration reaction and a cement-like behavior of the mechanically activated samples.

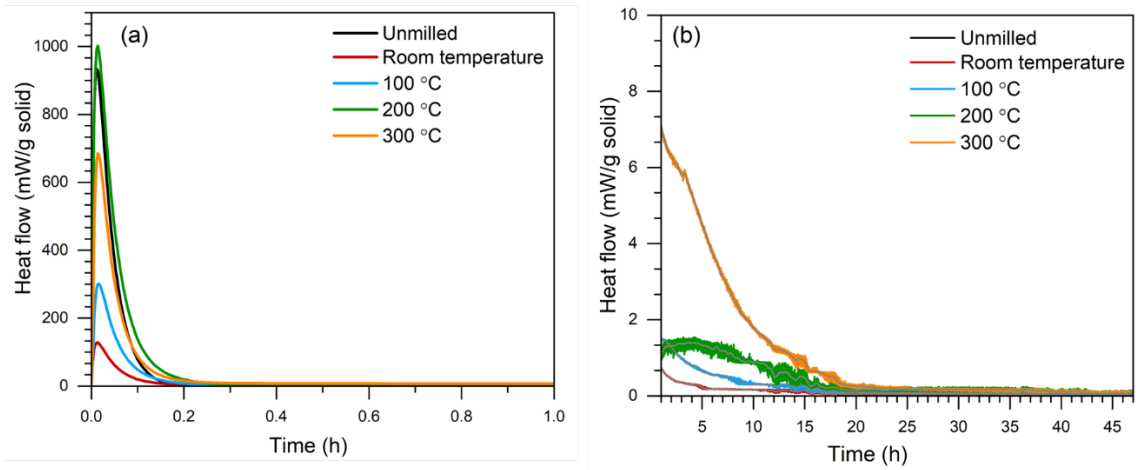

Figure 8: Heat flow calorimetry for the first (a) one hour of hydration and (b) up to 47 hours of hydration.

Figure 9 shows the TGA traces of each of the investigated samples. The hydration product $Ca(OH)_2$, as well as its carbonated form $CaCO_3$, were observed. Specifically, $Ca(OH)_2$ dehydroxylation is typically observed around 400-500 °C, while $CaCO_3$ decarbonation occurs between 650-750 °C. These could form through interaction of the CaO with water and CO_2 in air or could be formed from hydraulic reaction of calcium silicates, since portlandite is among the earliest hydration products formed in cement hydration. Another indicator of cement phase formation was the broad signal in the range from 60 to 300°C, with a more evident peak centered at ~120°C. This has been attributed to calcium silicate hydrate (C-S-H), the predominant product of cement hydration. The phase was more abundant in the samples subjected to milling at 300 °C. C-S-H exhibits water loss in the temperature range of 50-600 °C, due to the water loss present in the interlayer and dehydroxylation. Together, the identification of both main products of the hydration of calcium silicate cementitious phases suggests that a hydration of the amorphous calcium silicate phases occurred. This is a promising result for the application mechanochemical process for cement phase production.

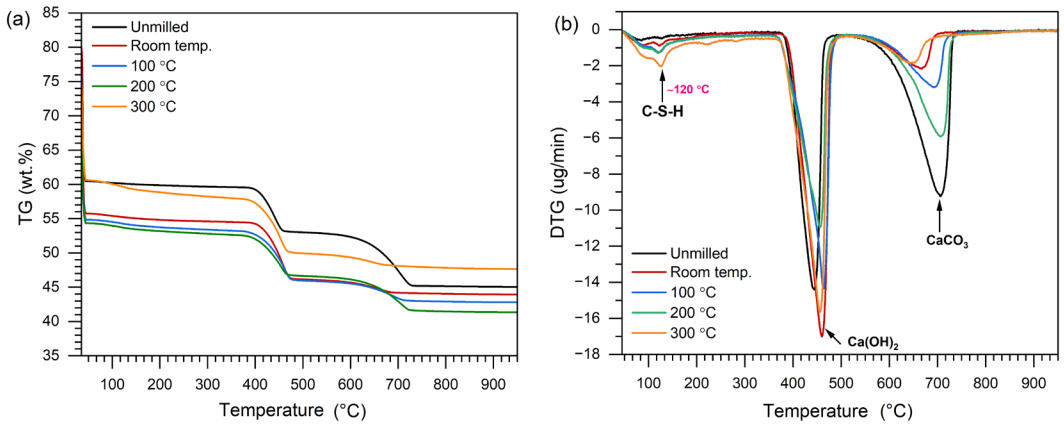

Figure 9: TGA results for the samples hydrated up to 47 hours. (a) weight loss as a function of the temperature and (b) DTG curve with all peaks assigned

4. Conclusion

Overall, thermal-assisted ball milling of the CaO/SiO_2 mixture results in enhanced formation of amorphous calcium silicate. With increasing the temperature of the milling process, the formation of Ca-O-Si bonds is promoted as illustrated by the DSC, ATR-FTIR, ^{29}Si MAS-NMR, and UV-Vis DRS. When annealed at 1000 °C, further crystallization of the material leads to the formation of calcium silicate phases such as β-C_2S, that are detectable by XRD. When the mixture is milled at 300 °C for 1 h, a high conversion of the initial CaO and SiO_2 crystals is achieved during subsequent annealing at 1000 °C, which was approximately 400 °C lower than conventional cement manufacturing. When mixed with water, the mixtures show hydration activity. The presence of cement hydration products such as CH and C-S-H is indicated by the TGA measurements, thus suggesting a hydration reaction and a cement-like behavior. These results suggest that the combination of the mechanical impacts in ball milling and elevated temperatures can create a favorable reaction environment toward a novel approach for production of hydraulic cement phases by converting solid SiO_2 and CaO through enhanced mixing, reactivity, as well further improving the solid-state diffusivity of both reagents.

Acknowledgment

VSN was funded by the U.S. Department of Energy, Office of Science, Office of Basic Energy Sciences, Chemical Sciences, Geosciences, and Biosciences Division under Award Number DE-SC0016486. XRD analysis was conducted at the Materials Characterization Facility (MCF) at Georgia Tech, supported by the GT Institute for Materials (IMat) and the Institute for Electronics and Nanotechnology (IEN), a member of the NSF-funded National Nanotechnology Coordinated Infrastructure (Grant ECCS-2025462). The authors express their gratitude to Dr. Johannes Leisen of the Georgia Tech NMR Laboratory for his support with the MAS NMR measurements. David Tavakoli from the Georgia Tech IEN/IMat Materials Characterization Facility is acknowledged for his help with the XRD measurements and the data analysis process. Erin V. Phillips is greatly acknowledged for the help in taking the SEM images. We thank Kinga M. Gołąbek and Letícia F. Rasteiro for their assistance in acquiring and data processing of the IR and UV-Vis spectra. We also extend our gratitude to Pawel Chmielniak, George Chang, and Bradley Parker for their assistance in designing the setup and running the experiments.

Author contributions

VSN: Conceptualization, investigation, data analysis, data visualization, method development, validation, writing - original draft, writing - review & editing. EQ: Conceptualization, investigation, data analysis, data visualization, validation, writing - review & editing. KNM: Investigation, validation.

DNG: Method development, JAD: Method development, KEK: Conceptualization, funding acquisition, method development, project administration, resources, supervision, writing - original draft, writing - review & editing, CS: Conceptualization, funding acquisition, method development, project administration, resources, supervision, writing - original draft, writing - review & editing.

References

1. Swercheck, A.; Ferguson, M.; Popoff, N.; Mack, J.; Lotito, G.; Deprimo, L.; Pontarollo, J., Roadmap to Carbon Neutrality. Portland Cement Association: 2021.
2. Worrell, E.; Martin, N.; Price, L., Potentials for energy efficiency improvement in the US cement industry. *Energy* **2000,** *25* (12), 1189-1214.
3. Khurana, S.; Banerjee, R.; Gaitonde, U., Energy balance and cogeneration for a cement plant. *Appl. Therm. Eng.* **2002,** *22* (5), 485-494.
4. Del Strother, P., *Lea's Chemistry of Cement and Concrete*. 2019; Vol. 1, p 31-56.
5. Sadighi, S.; Shirvani, M.; Ahmad, A., Rotary cement kiln coating estimator: Integrated modelling of kiln with shell temperature measurement. *Can. J. Chem. Eng.* **2011,** *89* (1), 116-125.
6. Salahudeen, N.; Ahmed, A. S.; Ala'a, H.; Dauda, M.; Waziri, S. M.; Jibril, B. Y., Synthesis of gamma alumina from Kankara kaolin using a novel technique. *Appl. Clay Sci.* **2015,** *105*, 170-177.
7. Botero, Y. L.; López-Rendón, J. E.; Ramírez, D.; Zapata, D. M.; Jaramillo, F., From clay minerals to Al2O3 nanoparticles: Synthesis and colloidal stabilization for optoelectronic applications. *Minerals* **2020,** *10* (2), 118.
8. Herfort, D.; Macphee, D. E., *Lea's Chemistry of Cement and Concrete*. 2019; p 57-86.
9. Legmann, H. In *Recovery of industrial heat in the cement industry by means of the ORC process*, IEEE-IAS/PCS 2002 Cement Industry Technical Conference. Conference Record (Cat. No. 02CH37282), IEEE: 2002; pp 29-35.
10. Zhang, G.; Zhu, G.; Wang, C. In *A New Application of Waste Heat Recovery Power Generation in Clinker Kiln*, 2009 IEEE Cement Industry Technical Conference Record, IEEE: 2009; pp 1-7.
11. Fujimoto, S., Modern technology impact on power usage in cement plants. *IEEE Trans. Ind. Appl.* **1994,** *30* (3), 553-560.
12. Akgun, F., Investigaton of energy saving and NOx reduction possibilities in a rotary cement kiln. *Int. J. Energy Res.* **2003,** *27* (4), 455-465.
13. Abdul-Wahab, S. A.; Al-Dhamri, H.; Ram, G.; Chatterjee, V. P., An overview of alternative raw materials used in cement and clinker manufacturing. *Int. J. Sustain. Eng.* **2021,** *14* (4), 743-760.
14. Baláž, P.; Achimovičová, M.; Baláž, M.; Billik, P.; Cherkezova-Zheleva, Z.; Criado, J. M.; Delogu, F.; Dutková, E.; Gaffet, E.; Gotor, F. J., Hallmarks of mechanochemistry: from nanoparticles to technology. *Chem. Soc. Rev.* **2013,** *42* (18), 7571-7637.
15. James, S. L.; Adams, C. J.; Bolm, C.; Braga, D.; Collier, P.; Friščić, T.; Grepioni, F.; Harris, K. D.; Hyett, G.; Jones, W., Mechanochemistry: opportunities for new and cleaner synthesis. *Chem. Soc. Rev.* **2012,** *41* (1), 413-447.
16. Takacs, L., The historical development of mechanochemistry. *Chem. Soc. Rev.* **2013,** *42* (18), 7649-7659.
17. Tricker, A. W.; Samaras, G.; Hebisch, K. L.; Realff, M. J.; Sievers, C., Hot spot generation, reactivity, and decay in mechanochemical reactors. *J. Chem. Eng.* **2020,** *382*, 122954.
18. Immohr, S.; Felderhoff, M.; Weidenthaler, C.; Schüth, F., An orders-of-magnitude increase in the rate of the solid-catalyzed CO oxidation by in situ ball milling. *Angew. Chem. Int. Ed.* **2013,** *52* (48), 12688-12691.
19. Yu, N.-K.; Rasteiro, L. F.; Nguyen, V. S.; Gołąbek, K. M.; Sievers, C.; Medford, A. J., Evaluating the Role of Metastable Surfaces in Mechanochemical Reduction of Molybdenum Oxide. *JACS Au* **2024,** *5* (1), 82-90.
20. Dodd, A.; McKinley, A.; Tsuzuki, T.; Saunders, M., Tailoring the photocatalytic activity of nanoparticulate zinc oxide by transition metal oxide doping. *Mater. Chem. Phys.* **2009,** *114* (1), 382-386.

21. He, R.; Hocking, R.; Tsuzuki, T., Local structure and photocatalytic property of mechanochemical synthesized ZnO doped with transition metal oxides. *J. Aust. Ceram.* **2013,** *49*, 70 - 75.
22. Tsuzuki, T., Mechanochemical synthesis of metal oxide nanoparticles. *Commun. Chem.* **2021,** *4* (1), 143.
23. Echresh, A.; Shoushtari, M. Z., Synthesis of Al-doping ZnO nanoparticles via mechanochemical method and investigation of their structural and optical properties. *Mater. Lett.* **2013,** *109*, 88-91.
24. Sabri, N. S.; Deni, M. S. M.; Zakaria, A.; Talari, M. K., Effect of Mn doping on structural and optical properties of SnO2 nanoparticles prepared by mechanochemical processing. *Phys. Procedia* **2012,** *25*, 233-239.
25. Gagrani, A.; Sousa, S.; Monteiro, O. C.; Tsuzuki, T., Solid state synthesis and photocatalytic activity of bio-inspired calcium manganese oxide catalysts. *J. Solid State Chem.* **2020,** *288*, 121390.
26. Gagrani, A.; Alsultan, M.; Swiegers, G. F.; Tsuzuki, T., Photo-electrochemical oxygen evolution reaction by biomimetic CaMn2O4 catalyst. *Appl. Sci.* **2019,** *9* (11), 2196.
27. Chen, G.-H., Mechanical activation of calcium aluminate formation from CaCO3–Al2O3 mixtures. *J. Alloys Compd.* **2006,** *416* (1-2), 279-283.
28. Mi, G.; Saito, F.; Hanada, M., Effects of Milling of a Mixture of Calcium Oxide and Silica-gel on Formation of Dicalcium Silicate by Heating and its Hydration. *Inorg. Mater.* **1997,** *4*, 591-595.
29. Stroh, J.; Ali, N. Z.; Maierhofer, C.; Emmerling, F., Ettringite via mechanochemistry: a green and rapid approach for industrial application. *ACS Omega* **2019,** *4* (4), 7734-7737.
30. Arteaga-Arcos, J. C.; Chimal-Valencia, O. A.; Delgado Hernández, D. J.; Yee Madeira, H. T.; de la Torre, S. D., High-Energy Ball Mill Parameters Used to Obtain Ultra-Fine Portland Cement at Laboratory Level. *ACI Mater. J.* **2011,** *108* (4).
31. Jicsinszky, L.; Rossi, F.; Solarino, R.; Cravotto, G., Comparison of the conventional and mechanochemical syntheses of cyclodextrin derivatives. *Molecules* **2023,** *28* (2), 467.
32. Zholdassov, Y. S.; Kwok, R. W.; Shlain, M. A.; Patel, M.; Marianski, M.; Braunschweig, A. B., Kinetics of primary mechanochemical covalent-bond-forming reactions. *RSC Mechanochem.* **2024,** *1* (1), 11-32.
33. Baki, V. A.; Ke, X.; Heath, A.; Calabria-Holley, J.; Terzi, C.; Sirin, M., The impact of mechanochemical activation on the physicochemical properties and pozzolanic reactivity of kaolinite, muscovite and montmorillonite. *Cem. Concr. Res.* **2022,** *162*, 106962.
34. Lee, J.; Lothenbach, B.; Moon, J., Performance improvement of Portland-limestone cement by mechanochemical activation. *Cem. Concr. Res.* **2024,** *176*, 107411.
35. Sheng, D.; Lan, J.; Du, Z.; Ma, Y.; Zhou, M.; Hou, H., Preparation of cementitious materials from mechanochemically modified copper smelting slag compounded with high-aluminum fly ash. *Materials* **2024,** *17* (3), 546.
36. Xu, M.; Guo, L.; Wen, J.; Hu, X.; Wang, L.; Mo, L., Mechanochemical Activation of Basic Oxygen Furnace Slag: Insights into Particle Modification, Hydration Behavior, and Microstructural Development. *Materials* **2025,** *18* (15), 3687.
37. Muzenda, T. R.; Georget, F.; Matschei, T., Mechano-chemical activation of kaolins–Effect of mineral composition and triethanolamine on activation effectiveness and hydration. *Constr. Build. Mater.* **2025,** *482*, 141703.
38. Yusuf, M. O., Bond characterization in cementitious material binders using Fourier-transform infrared spectroscopy. *Appl. Sci.* **2023,** *13* (5), 3353.
39. Iftiquar, S., Structural studies on semiconducting hydrogenated amorphous silicon oxide films. *High Temp. Mater. Process.* **2002,** *6* (1).
40. Rodriguez-Blanco, J. D.; Shaw, S.; Benning, L. G., The kinetics and mechanisms of amorphous calcium carbonate (ACC) crystallization to calcite, via vaterite. *Nanoscale* **2011,** *3* (1), 265-271.
41. Ren, X.; Zhang, W.; Ye, J., FTIR study on the polymorphic structure of tricalcium silicate. *Cem. Concr. Res.* **2017,** *99*, 129-136.
42. Ashraf, W.; Olek, J., Carbonation behavior of hydraulic and non-hydraulic calcium silicates: potential of utilizing low-lime calcium silicates in cement-based materials. *J. Mater. Sci.* **2016,** *51*, 6173-6191.

43. Walkley, B.; Provis, J., Solid-state nuclear magnetic resonance spectroscopy of cements. *Mater. Today Adv.* **2019,** *1*, 100007.
44. Skibsted, J.; Jakobsen, H. J.; Hall, C., Quantification of calcium silicate phases in Portland cements by 29 Si MAS NMR spectroscopy. *J. Chem. Soc. Faraday Trans.* **1995,** *91* (24), 4423-4430.
45. Scrivener, K.; Snellings, R.; Lothenbach, B., *A practical guide to microstructural analysis of cementitious materials*. Crc Press Boca Raton, FL, USA:: 2016; Vol. 540, p 213-287.
46. Makuła, P.; Pacia, M.; Macyk, W., How to correctly determine the band gap energy of modified semiconductor photocatalysts based on UV–Vis spectra. *J. Phys. Chem. Lett.* **2018,** *9* (23), 6814-6817.
47. Chesley, J.; Burnet, G., A two-stage reaction sequence for C3S formation. *Cem Concr Res.* **1989,** *19* (6), 837-847.
48. Kim, D., Effect of Adjusting for Particle-Size Distribution of Cement on Strength Development of Concrete. *Adv. Mater. Sci. Eng.* **2018,** *2018* (1), 1763524.
49. Zhang, Y.; Napier-Munn, T., Effects of particle size distribution, surface area and chemical composition on Portland cement strength. *Powder Technol.* **1995,** *83* (3), 245-252.
50. Innocenti, G.; Benkeser, D. J.; Dase, J. E.; Wirth, X.; Sievers, C.; Kurtis, K. E., Beneficiation of ponded coal ash through chemi-mechanical grinding. *Fuel* **2021,** *299*, 120892.
51. Katsioti, M.; Tsakiridis, P.; Giannatos, P.; Tsibouki, Z.; Marinos, J., Characterization of various cement grinding aids and their impact on grindability and cement performance. *Constr. Build. Mater.* **2009,** *23* (5), 1954-1959.